JACS
JOURNAL OF THE AMERICAN CHEMICAL SOCIETY

ARTICLE

pubs.acs.org/JACS

Continuous Lipid Bilayers Derived from Cell Membranes for Spatial Molecular Manipulation

Lisa Simonsson, Anders Gunnarsson, Patric Wallin, Peter Jönsson, and Fredrik Höök*

Department of Applied Physics, Chalmers University of Technology, SE 41296 Gothenburg, Sweden

Supporting Information

ABSTRACT: Progress with respect to enrichment and separation of native membrane components in complex lipid environments, such as native cell membranes, has so far been very limited. The reason for the slow progress can be related to the lack of efficient means to generate continuous and laterally fluid supported lipid bilayers (SLBs) made from real cell membranes. We show in this work how the edge of a hydrodynamically driven SLB can be used to induce rupture of adsorbed lipid vesicles of compositions that typically prevent spontaneous SLB formation, such as vesicles made of complex lipid compositions, containing high cholesterol content or being derived from real cell membranes. In particular, upon fusion between the moving edge of a preformed SLB and adsorbed vesicles made directly from 3T3 fibroblast cell membranes, the membrane content of the vesicles was shown to be efficiently transferred to the SLB. The molecular transfer was verified using cholera toxin B subunit (CTB) binding to monosialoganglioside receptors (G_{M1} and G_{M3}), and the preserved lateral mobility was confirmed by spatial manipulation of the $G_{M1/M3}$−CTB complex using a hydrodynamic flow. Two populations of CTB with markedly different drift velocity could be identified, which from dissociation kinetics data were attributed to CTB bound with different numbers of ganglioside anchors.

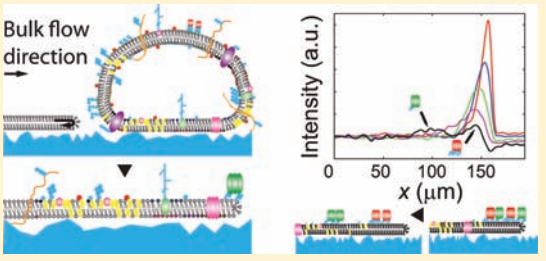

INTRODUCTION

The cell membrane is built up by several different types of lipids and proteins and fulfills the role of separating the cell interior from its surrounding environment. Simultaneously, it is responsible for selective translocation of a multitude of molecular signals across the membrane. A key property of the cell membrane is its two-dimensional fluidity,[1] which allows for the molecular building blocks to diffuse laterally into functional supramolecular architectures.[2] The emerging view is that local arrangements of lipids and proteins play central roles for many biological functions. For instance, the local lipid environment has been proposed to control membrane protein activity,[3] fine-tune processes like endo- and exocytosis[4] and cell signaling,[5] and facilitate viral entry.[6] The cell membrane is also hosting the majority of pharmaceutical drug targets, which has further contributed to the extensive research currently devoted to reach an in-depth understanding of the cell membrane.[7]

Facilitated by the increasing information content offered by surface-based techniques, such as scanning probe techniques,[8] electrical impedance spectroscopy,[9] fluorescence imaging,[10] quartz crystal microbalance,[11] surface plasmon resonance,[12] etc., planar supported lipid bilayers (SLBs) have emerged as one of the most important mimics of the natural cell membrane.[13] One particularly attractive feature of SLBs is their lateral fluidity, which has been extensively explored as a means to separate and isolate membrane-associated molecules.[14−18] However, the current lack of methods to generate planar and laterally fluid SLBs derived directly from cell membranes has obstructed the ultimate goal of such attempts, being detergent-free isolation of cell membrane-associated molecules while in their native lipid environment.

The most popular strategy used to form SLBs is via lipid vesicle adsorption, which under certain solution conditions can result in spontaneous SLB formation on a few selective surfaces (typically SiO_2, TiO_2, or mica).[19,20] However, due to a delicate balance between surface adhesion and vesicle−vesicle interactions, this process is spontaneous[21,22] for a very limited range of lipid compositions. For example, addition of a large fraction of cholesterol (≥40 mol %) prevents SLB formation on otherwise very potent SiO_2 surfaces.[23] Other examples are the addition of lipids in the gel phase[24] and the addition of lipids with negative curvature,[25] proteoliposomes,[26,27] and lipid vesicles composed of *Escherichia coli* lipids.[21] Although lipid vesicles with complex compositions can be forced to form SLBs using various tricks, such as the addition of divalent ions like Ca^{2+}(ref 28), osmotic stress,[29] and raised temperature,[28] often in combination with very long (3−7 h) incubation times,[28,29] there are many other situations for which SLB formation is still prevented. In particular, the challenge of generating continuous SLBs directly from native cell membranes[30] or transfer of natural cell membrane components into SLBs remains essentially unsolved.

A particularly versatile and attractive way of handling SLBs is offered by progress in microfluidics.[31,32] We recently

Received: May 19, 2011
Published: July 25, 2011

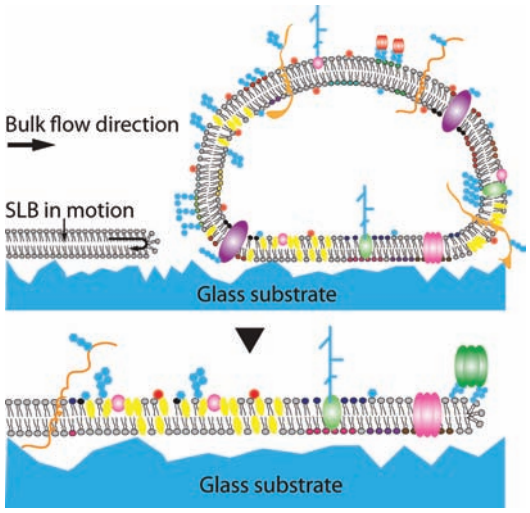

Figure 1. Concept illustration: The front edge of the SLB is driven toward a cell membrane-derived lipid vesicle using a hydrodynamic force that is induced using a liquid bulk flow (top). Upon contact, the lipid vesicle ruptures and is incorporated into the SLB (bottom).

demonstrated that the hydrodynamic shear force from a liquid flow above a SLB formed in a microfluidic channel can be used to move the entire SLB in the direction of the flowing liquid,[33] with the edge of the SLB obeying a rolling type motion. Furthermore, it was shown that the SLB edge acts as a nanoscale sieve, enabling membrane-bound proteins to be accumulated at orders of magnitude increased surface concentrations. It was also demonstrated that different types of membrane-bound molecules could be separated based on differences in drift velocity, as in conventional chromatography, but without the need of first extracting the molecules of interest from the lipid bilayer. In this work, we demonstrate how a hydrodynamically driven edge of an SLB can be used to collapse and merge with adsorbed and stationary lipid vesicles positioned in front of the energetically unfavorable SLB edge. In this way, adsorbed lipid vesicles of complex lipid compositions can be converted into a SLB, as schematically illustrated in Figure 1.

Vesicles of complex molecular compositions that do not spontaneously form SLBs upon adsorption on SiO_2, characterized by high ($\geq$40 mol %) cholesterol content or being derived directly from cell membranes (3T3 fibroblast), have been investigated. Transfer and sustained lateral mobility of cell membrane components was investigated by enriching and separating populations of cholera toxin bound to ganglioside lipids.

MATERIALS AND METHODS

Materials. The 1-palmitoyl-2-oleoyl-*sn*-glycero-3-phosphocholine (POPC), 1,2-dioleoyl-*sn*-glycero-3-phosphocholine (DOPC), 1,2-dioleoyl-*sn*-glycero-3-phosphoethanolamine (DOPE), and cholesterol were purchased from Avanti Lipids Inc., Alabaster, AL. Lissamine rhodamineB 1,2-dihexadecanoyl-*sn*-glycero-3-phosphoethanolamine (rhodamine-DHPE, $\lambda_{exc.}/\lambda_{em.}$ = 560/580 nm) was purchased from Molecular Probes, Eugene, OR.The 2(12-(7-nitrobenz-2-oxa-1,3-diazol-4-yl)amino)dodecanoyl-1-hexadecanoyl-*sn*-glycero-3-phosphocholine (NBD C_{12}-HPC, $\lambda_{exc.}/\lambda_{em.}$ = 463/536 nm) was purchased from Invitrogen, Carlsbad, CA. Tris(hydroxymethyl)-aminomethane hydrochloride (Tris) was from VWR International, Stockholm, Sweden. Cholera toxin B subunit-fluorescein isothiocyanate conjugate (CTB, $\lambda_{exc.}/\lambda_{em.}$ = 494/519 nm), neutravidin, sodium chloride (NaCl), ethylenediaminetetraacetic acid (EDTA), sodium dodecyl sulfate (SDS), methanol, and chloroform were from Sigma Aldrich, Steinheim, Germany. Hydrogen peroxide and ammonium hydroxide were from Fisher Scientific, Västra Frölunda, Sweden. Hydrogen chloride (HCl) was from Merck, Darmstadt, Germany.

Preparation of Artificial and Native Lipid Vesicles. Vesicles were composed of POPC, DOPC/cholesterol (60:40 mol % and 50:50 mol %), and DOPC/DOPE/cholesterol (39:21:40 mol %). POPC vesicles were fluorescently labeled with 0.1 or 1 wt % NBD C_{12}-HPC. DOPC/cholesterol and DOPC/DOPE/cholesterol vesicles were fluorescently labeled with 1 wt % of rhodamine-DHPE. Lipids were dissolved in a 1:1 chloroform/methanol mixture. Lipid vesicles were prepared by evaporation of the solvent under N_2 (>1 h), followed by hydration in buffer (10 mM of Tris/HCl, pH of 8.0, 100 mM of NaCl, and 1 mM of EDTA) for >30 min, followed by extrusion through 30 nm polycarbonate membranes (Whatman, Maidstone, U.K.) 11 times. The total lipid concentrations were 0.5−3 mg/mL, depending on lipid composition. The lipid vesicle suspensions were stored at 4 °C. The lipid vesicles were diluted with buffer solution (10 mM of Tris/HCl, pH of 7.4, 100 mM of NaCl, and 1 mM of EDTA) to a total lipid concentration of 0.1 mg/mL prior to each experiment.

Cell membrane-derived vesicles were made by incubating 3T3 fibroblast cells with rhodamine-DHPE labeled (1 wt %) POPC vesicles, leading to lipid uptake by the cells and consequently labeling of their membranes. Vesicles were made from cell membrane fragments by extruding the labeled cells through 800 nm followed by 200 nm polycarbonate membranes using an Avanti mini extruder (Avanti polar lipids, Alabaster, AL). Water-soluble proteins were removed using ultracentrifugation (Beckman Coulter, Brea CA) and filtering using centrifugal filters (Amicon Ultra −0.5 mL 100 K, Millipore, Carrigtwohill, Co. Cork, Ireland). The size distribution of the cell membrane derived vesicles was measured using a nanoparticle tracking analyzer (NanoSight, U.K.). The average diameter was determined to 150 ± 30 nm.

Fluorescence Microscopy. The fluorescently labeled molecules were studied with an inverted Nikon Eclipse Ti-E microscope (Nikon Corporation, Tokyo, Japan), using an Andor iXon+ EMCCD camera (Andor Technology, Belfast, Northern Ireland) and a 60 × magnification (NA = 1.49) oil immersion objective (Nikon Corporation). The acquired images consisted of 512 × 512 pixels with a pixel size of 0.38 × 0.38 μm. To monitor the fluorescent molecules, a mercury lamp connected to the microscope using an optical fiber (Intensilight C-HGFIE; Nikon Corporation) was used together with a TRITC (rhodamine-DHPE) or a FITC (NBD-PC and CT) filter cube (Nikon Corporation), depending on the dye studied. All data generation was done using time-lapse acquisition, with an exposure time of 100 ms. In the experiments with NBD-PC in the SLB and rhodamine-DHPE in the adsorbed lipid vesicles, one image was first taken using a FITC filter cube, immediately followed by an image taken using a TRITC filter cube.

RESULTS AND DISCUSSION

Fusion of Lipid Vesicles with High Cholesterol Content. Fusion between adsorbed lipid vesicles and the moving edge of an SLB made from POPC was used to generate an SLB with lipid compositions that typically prevent spontaneous SLB formation upon vesicle adsorption on SiO_2. This was done by driving the preformed SLB made from POPC against adsorbed nonruptured lipid vesicles composed of: (1) DOPC:cholesterol (60:40 mol %), (2) DOPC:cholesterol (50:50 mol %), and (3) DOPC:DOPE:cholesterol (39:21:40 mol %).

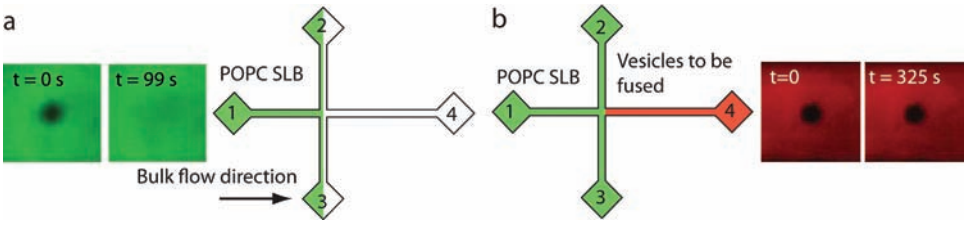

Figure 2. Sketches of the microfluidic channel at different stages of the experiments. (a) A POPC SLB, dye labeled with NBD C_{12}-HPC (green), formed in the left part of the channel. Also shown are micrographs of a photobleached spot in the SLB and the recovery after 99 s, used for fluorescence recovery after photobleaching (FRAP) analysis of the diffusivity of the SLB. The numbers (1−4) indicate the indexing of the in- and outlets of the 4-arm channel. (b) The NBD-labeled (green) SLB driven forward in the microfluidic channel and DOPC/CH (60:40 mol %) vesicles, dye labeled with rhodamine-DHPE (red), adsorbed to the floor of channel 4. The adsorbed vesicles remained nonruptured as shown by fluorescence recovery after photobleaching (FRAP). The fabrication of the microfluidic cross channel is detailed in the Supporting Information.

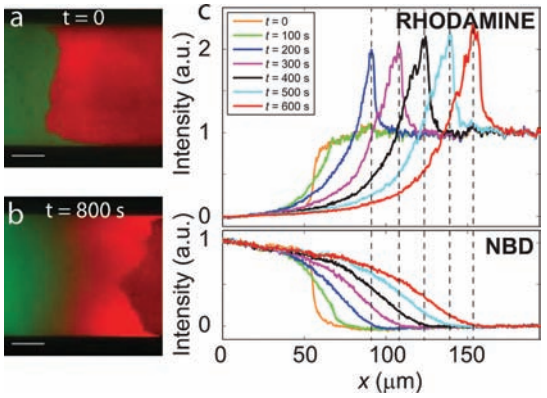

Figure 3. (a and b) Merged micrographs of a NBD-labeled POPC SLB (green) driven toward rhodamine-labeled DOPC/CH vesicles (red), before onset of the bilayer motion (t = 0) and after interrupted bilayer motion (t = 800 s). (c) Time evolution in steps of 100 s for the median values of the line intensity along the center of the microfluidic channel for the two color channels, rhodamine (top) and NBD (bottom). The curves in (c) were obtained by subtracting the intensity for each line profile with the intensity at the far left of the line profile, followed by normalization with the intensity at the far right. (Scale bar represents 40 μm).

A T-shaped SLB was generated in the left-hand part of a microfluidic cross channel (Figure 2a) by flowing (10 μL/min) a POPC vesicle suspension (0.1 mg/mL of POPC labeled with 1 wt % of NBD C_{12}-HPC from channel arm 1 to channel arms 2 and 3, while simultaneously having a flow of pure buffer (20 μL/min) from channel arm 4 to channel arms 2 and 3. Fluorescence recovery after photobleaching (FRAP)[34] showed full recovery of the SLB made from POPC with a diffusivity of 2.2 ± 0.2 $\mu m^2 s^{-1}$ (n = 3) and an immobile fraction of <1% (Figure 2a). The shear force induced from a more than ten times higher bulk flow (250 μL/min) was subsequently used to drive the SLB in the direction from channel arm 1 to 4, while keeping channel arms 2 and 3 closed (Figure 2b). The resulting speed of the bilayer front was estimated to ∼0.2 μm/s, corresponding to an exerted force per surface area of ∼20 Pa.[35] Lipid vesicles labeled with 1 wt % rhodamine-DHPE (Figure 2b, red) of lipid composition 1, 2, or 3 were subsequently adsorbed in front of the POPC SLB. This was done by adding the vesicle suspension (0.1 mg/mL) at a flow speed of 20 μL/min from channel arm 1 to 4. At this flow, the SLB remains stationary and prevents vesicle adsorption on the region it covers. The adsorbed vesicles of compositions 1, 2, and 3 displayed no fluorescence recovery after photobleaching, which is shown for (1) in Figure 2b. This is consistent with adsorption of nonruptured vesicles, as also supported by quartz crystal microbalance data (see Supporting Information). In agreement with previous observations,[33] a constant motion of the SLB front could be induced by subsequently increasing the flow speed from channel arm 1 to 4 to 250 μL/min, while the adsorbed lipid vesicles were observed to remain stationary.

The interaction between the front edge of the moving SLB (green in Figure 3a) and the adsorbed lipid vesicles (red in Figure 3a) was followed in real time (see video 1, Supporting Information) using total internal reflection fluorescence (TIRF) microscopy. Essentially identical results to those shown in Figure 3 were obtained for vesicles of lipid compositions 2 and 3 (see Supporting Information).

Figure 3a and b shows TIRF micrograph snapshots of the process at t = 0 and 800 s (Figure 3a and b, respectively). At t = 0, there is a sharp border between the green and the red intensities. At t = 800 s, the sharp border between green and red has become dim, and there is an increase in the red intensity at the front of the lipid bilayer. The latter observation is attributed to a combination of: (i) adsorbed vesicles that have collapsed into a planar configuration, thus bringing the dye-labeled lipids into a region of the TIRF illumination with higher excitation light intensity and (ii) rhodamine-DHPE lipids that have been transferred to and accumulated at the front of the moving SLB, as previously observed for rhodamine-DHPE labeled SLBs under shear-driven motion.[33] These observations suggest that the adsorbed nonruptured vesicles of lipid composition (1) have fused with the moving edge of the SLB to form a planar SLB containing a mixture of the green and the red labels. This interpretation is further supported by FRAP measurements performed over the border region, demonstrating full recovery for rhodamine-DHPE to the left of the border, with a diffusivity comparable to that of NBD-PC and no recovery to the right of the border (see video 2, Supporting Information).

Additional details regarding the fusion process can be revealed by analyzing the temporal variation of the intensity profiles of the two dyes along the microfluidic channel. Figure 3c shows median values of the fluorescence intensity from rhodamine-DHPE (top) and NBD-PC (bottom) taken over 50 pixels in the y-direction (perpendicular to the channel direction) at the center of the channel. The intensity from rhodamine-DHPE in the front of the SLB increases with time to more than twice the intensity of the intact vesicles. This is, as explained above, attributed to accumulation of rhodamine-DHPE lipids at the front of the bilayer. The intensity gradient along the channel represents evidence for diffusion of rhodamine-DHPE backward, against the direction of SLB motion, and hence mobility of rhodamine-DHPE

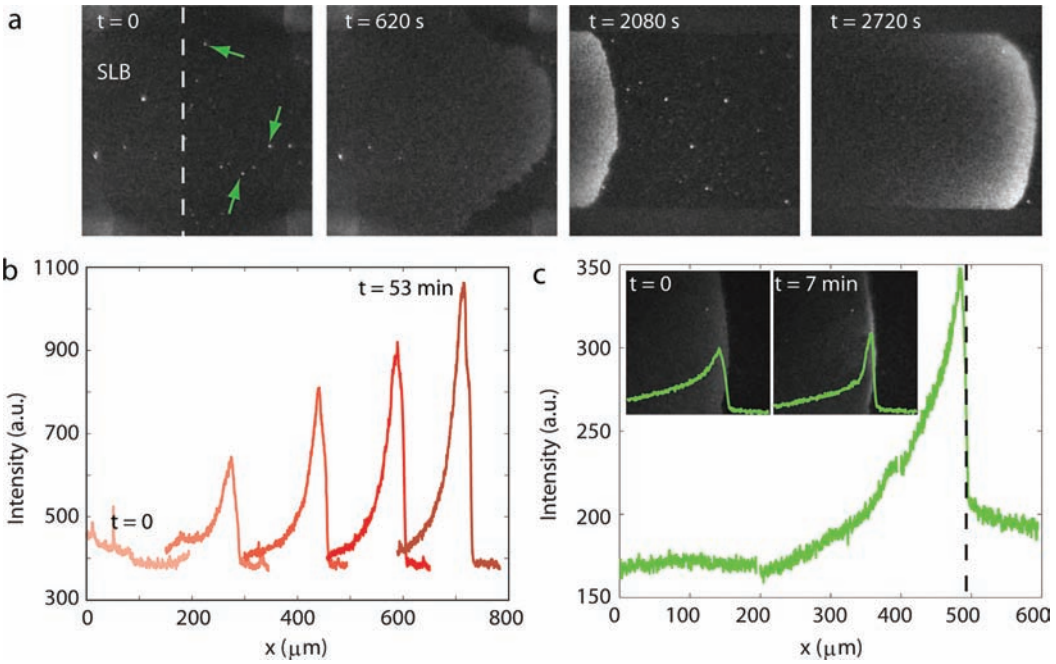

Figure 4. (a) Time series of micrographs of an unlabeled POPC SLB driven with a buffer flow of 250 μL/min against rhodamine-DHPE labeled cell membrane-derived vesicles that were adsorbed in front of the SLB. The white dashed line indicates the location of the SLB front prior to the start of SLB motion. The arrows indicate some of the adsorbed cell membrane-derived vesicles. (b) Average intensity from transferred rhodamine-DHPE along the microfluidic channel for the data shown in (a). (c) Average intensity along the microfluidic channel after binding of fluorescently labeled CTB (320 nM) followed by rinsing at 20 μL/min. The dashed line in (c) indicates the bilayer front. The insets are micrographs of the CTB-containing SLB front before and after 7 min of flowing buffer at 250 μL/min. The green lines in the insets correspond to the average fluorescence intensity along the microfluidic channel. The glass surface in front of the SLB was passivated using neutravidin (20 μg/mL) to prevent CTB from binding unspecifically to the glass surface. The neutravidin also acted as a barrier, which hindered the SLB from moving further in the forward direction.

in the SLB. The bottom graph shows the time evolution of the intensity from NBD-PC, displaying motion of NBD-PC to the right and depletion of NBD-PC in the front. A likely explanation to the depletion in the front is that NBD-PC moves slower than rhodamine-DHPE in the moving SLB, which is in agreement with previous studies.[33] Fluorescence resonance energy transfer (FRET) between NBD-PC and rhodamine-DHPE may also contribute to the decline in intensity. Interestingly, the complete depletion of NBD-PC in the very front of the SLB indicates that the lipid composition is in this region mainly determined by the lipid composition of the fused vesicles. However, due to lipid diffusion this is a transient state, which means that quantitative conclusions regarding the actual lipid composition cannot be made without using labels that do not influence the motion of the lipids. We stress, however, that a flow of, e.g., detergents could potentially be used to remove the lipid reservoir after completed fusion. This would in turn generate a SLB of a lipid composition essentially identical to that of the adsorbed vesicles.

The underlying mechanism of how the driven SLB collapses and merges with the adsorbed vesicles is still not fully understood. It has previously been concluded experimentally that the inherent instability of the SLB edge is sufficient to induce vesicle rupture.[36] In addition, the fusion process is thermodynamically favorable according to theory,[36,37] but most likely there is an energy barrier that must be overcome. The latter assumption is supported by the fact that the velocity of the bilayer front as it fuses vesicles was estimated to 0.17 μm/s, which corresponds to a slight reduction in comparison with an SLB driven on a bare glass surface (0.2 μm/s). Although a thorough theoretical investigation of the mechanism behind the hydrodynamically induced vesicle fusion is beyond the scope of this work, there are several possible explanations to why adsorbed vesicles that do not spontaneously form an SLB can be fused into an SLB in this manner. For example, the edge of the moving lipid bilayer may lower the energy barrier of rupturing a vesicle. In addition, if a vesicle is not fused to the SLB, the lipid bilayer needs to circumvent the vesicle, thus creating a pore in the lipid bilayer. This state, however, is energetically unfavorable, since it exposes the hydrophobic lipid tails to the aqueous solution. A third plausible scenario, in addition to the two mentioned above, is that adsorbed vesicles are peeled off by the moving SLB. However, the high efficiency of rhodamine-DHPE transfer suggests that this is a very rare process.

Incorporation of Native Cell Membrane Components into SLBs. To further investigate the capacity of the concept, the possibility to generate an SLB containing native cell-membrane components was explored. This was done by driving the edge of a SLB made from POPC against adsorbed and nonruptured cell membrane-derived vesicles. The procedure described above was repeated, with the exception that the adsorbed lipid vesicle was replaced with vesicles derived directly from rhodamine-DHPE stained cell membranes of 3T3 fibroblasts. Figure 4a shows micrographs of an unlabeled SLB made from POPC, the edge of which being driven against stationary cell membrane-derived vesicles. In analogy with the results shown in Figure 3, rhodamine-DHPE becomes accumulated at the front of the moving SLB (Figure 4a and b), confirming that lipid material was successfully transferred from the vesicles to the moving SLB. (See also video 3, Supporting Information, illustrating a fusion efficiency of around 80%).

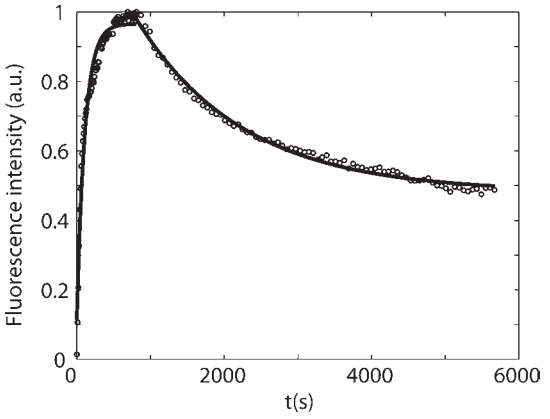

Figure 5. Binding and release kinetics of CTB interacting with $G_{M1/M3}$ from time-resolved TIRF microscopy. The circles are data points, and the black lines are exponential fits to $A_1(1 - \exp(-(C_{ligand}k_{on} + k_{off})t)) + C_1$ and $A_2 \exp(-k_{off}t) + C_2$ for the binding and release, respectively.

To verify successful incorporation of native cell membrane constituents into the SLB, fluorescein conjugated CTB was used to identify the presence of monosialoganglioside G_{M1} (and possibly G_{M3}) lipids, which are known to be present in the outer membrane of 3T3 fibroblast cells.[38] Upon addition of CTB, preferential binding was observed at the front of the SLB (Figure 4c), demonstrating that $G_{M1/M3}$ lipids were accumulated in the front of the bilayer. By increasing the flow rate to 250 μL/min after saturated binding of CTB, further enrichment of $G_{M1/M3}$−CTB complexes at the bilayer front was observed (inset micrographs at $t = 0$ and 7 min in Figure 4c). This observation is attributed to the larger hydrodynamic force exerted on a $G_{M1/M3}$−CTB complex compared to that of the lipid molecules in the SLB, as a result of the large CTB molecule protruding into the bulk solution.[18] The accumulation of the $G_{M1/M3}$−CTB complex also demonstrates that lateral mobility is preserved, thus providing a detergent-free way to locally enrich low-abundant cell membrane components while remaining in their native lipid bilayer environment.

Binding Kinetics and Spatial Manipulation of CTB Populations Bound to a Cell Membrane SLB. The evanescent illumination of TIRF microscopy enables time-resolved measurements of CTB binding to and releasing from the SLB (Figure 5). After compensating for bleaching, the binding and release data were fitted according to the Langmuir binding model (see Supporting Information for details).

The average rate constants were found to be $k_{on} = 40 \times 10^3 \pm 17 \times 10^3\ M^{-1}\ s^{-1}$ ($n = 2$) and $k_{off} = 7.7 \times 10^{-4} \pm 1.1 \times 10^{-4}\ s^{-1}$ ($n = 3$), and the average dissociation constant was $K_D = 22$ nM ± 12 nM. The value of k_{off} is in the expected range of the CTB−G_{M1} interaction, whereas k_{on} is slower than CTB binding to artificial G_{M1} systems,[39] possibly due to mass transport limitations. Interestingly, while around 50% of the CTB−$G_{M1/M3}$ complexes dissociate within the time scale of the measurement, additional fractions appear irreversibly bound on these time scales (Figure 5). This is in agreement with previous studies of CTB binding to G_{M1},[39] generally attributed to the ability of CTB to establish multiple (up to five) bonds to G_{M1}. The good agreement with a single exponential curve for the dissociation trace suggests that in this case, one fraction of the CTB−$G_{M1/M3}$ complex has established sufficiently few bonds to yield a measurable dissociation rate, possibly also influenced by different binding strengths to G_{M1} and G_{M3}.

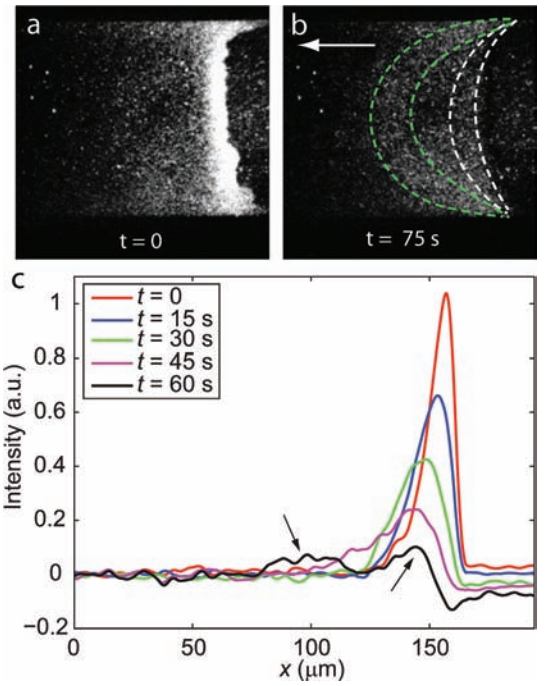

Figure 6. (a and b) Micrographs of CTB accumulated in the front of a cell membrane-derived SLB before ($t = 0$) and after ($t = 75$ s) onset of a reversed flow (the arrow indicates the flow direction). (c) Line profiles of the intensity from the mobile $G_{M1/M3}$−CTB complex along the center of the microfluidic channel at different times after a flow of 250 μL/min is being applied from right to left.

While this type of information on protein binding kinetics can be easily obtained by numerous methods, the ability to manipulate the motion of membrane-bound molecules using a hydrodynamic flow provides a means to confirm this hypothesis. By changing the direction of the motion of the CTB−$G_{M1/M3}$ complex by simply reversing the flow after accumulation at the front of the SLB, as shown previously for an artificial SLB-containing CTB−$G_{M1/M3}$ complexes,[18] two fluorescent bands of similar intensity were observed to move with significantly different drift velocities (Figure 6 and video 4, Supporting Information).

In order to more clearly visualize the two $G_{M1/M3}$−CTB populations, the intensity along the center of the channel, normalized with the background intensity, was plotted versus time (Figure 6c). The drift velocities of the fast and slow bands were estimated to ~1 and ~0.14 μm/s, respectively, at a bulk flow of 250 μL/min. These values are around a factor of 4 lower than previously observed for artificial SLBs containing 0.01 wt % of G_{M1}.[18] This observation can be due to steric hindrance originating from the complex mixture of lipids and proteins from the native cell membrane or from a larger number of anchors per CTB molecule. The drift velocity of a membrane-bound molecule is a balance between the force exerted on the protruding part of the molecule and the friction experienced from the coupling to the SLB. Under the reasonable assumption that the structure of CTB is not significantly influenced by the number of bonds established to the $G_{M1/M3}$ lipids, the two populations most likely represent complexes with different numbers of $G_{M1/M3}$ anchors, a view that is fully consistent with the interpretation of the kinetic data. As seen in Figure 6c, some of the CTB intensity is lost with time. This decrease is attributed to loss of bound CTB upon rinsing (see kinetic data in Figure 5).

CONCLUSIONS

Until now, formation of planar SLBs derived directly from cell membranes has, to our knowledge, been limited to micrometer-sized membrane patches formed on cellulose films, where no lateral mobility of membrane-bound proteins could be observed.[40] Using the concept presented in this work, continuous and laterally mobile supported lipid membranes can be achieved on plain glass surfaces, not only for real cell membranes but also for several other lipid compositions which do not easily convert into planar SLBs. The preserved lateral mobility of SLBs containing native cell membrane components made it possible to realize two-dimensional manipulation, such as accumulation and separation of biomolecules in their native lipid environment. Local enrichment of membrane-bound molecules is particularly interesting in the context of probing ligand and drug interactions with membrane-bound receptors, in which case the surface concentration is typically too low to yield sufficient signal-to-noise for label-free studies using surface plasmon resonance[12] and imaging mass spectrometry.[41] The method may also be applicable to manipulate transmembrane proteins, which typically appear immobile in SLBs. In previous work, we have shown that SLBs can be driven across substrates that do not promote spontaneous SLB formation.[42] By driving the SLB over a substrate that provides a sufficient lipid adhesion, while simultaneously promoting lateral motion of transmembrane proteins using, e.g., polymer cushions, we anticipate that the concept presented in this work could be a first step towards realizing the important challenge of enriching and separating also transmembrane proteins. The possibility to use a hydrodynamic flow to manipulate an SLB in the way described in this work puts restrictions on the height of the channel, which should be on the order of 100 μm or less to allow operation at reasonable flow speeds. However, the width of the channel(s) can easily be increased to macroscopic dimensions, which implies that future upscaling of membrane protein enrichment and separation is not excluded. Altogether, the possibility of forming and manipulating lipid bilayers that better mimic real cell membranes may contribute to bridge the gap between studies of simplistic mimics of the cell membrane and studies on live cells.

ASSOCIATED CONTENT

Supporting Information. Details for fabrication and experimental procedures for moving the SLB and fusing vesicles, interaction kinetics, accumulation, separation, FRAP, and QCM-D. This material is available free of charge via the Internet at http://pubs.acs.org.

AUTHOR INFORMATION

Corresponding Author
fredrik.hook@chalmers.se

ACKNOWLEDGMENT

This work was financially supported by the Swedish Research Council for Engineering Sciences, contract no. 2010-5063, the FFL grant from the Strategic Research Foundation, and VINNOVA.

REFERENCES

(1) Singer, S. J.; Nicolson, G. L. *Science* **1972**, *175*, 720.
(2) Edidin, M. *Annu. Rev. Biophys. Biomol. Struct.* **2003**, *32*, 257.
(3) Boesze-Battaglia, K.; Schimmel, R. J. *J. Exp. Biol.* **1997**, *200*, 2927.
(4) Mizunokamiya, M.; Inokuchi, H.; Kameyama, Y.; Yashiro, K.; Shin, S. O.; Fujita, A. *J. Biochem.* **1995**, *118*, 693.
(5) Simons, K.; Ikonen, E. *Nature* **1997**, *387*, 569.
(6) Kapadia, S. B.; Barth, H.; Baumert, T.; McKeating, J. A.; Chisari, F. V. *J. Virol.* **2007**, *81*, 374.
(7) Edidin, M. *Nat. Rev. Mol. Cell Biol.* **2003**, *4*, 414.
(8) Binnig, G.; Quate, C. F.; Gerber, C. *Phys. Rev. Lett.* **1986**, *56*, 930.
(9) Katz, E.; Willner, I. *Electroanalysis* **2003**, *15*, 913.
(10) Thompson, N. L.; Pearce, K. H.; Hsieh, H. V. *Eur. Biophys. J.* **1993**, *22*, 367.
(11) Rodahl, M.; Hook, F.; Krozer, A.; Brzezinski, P.; Kasemo, B. *Rev. Sci. Instrum.* **1995**, *66*, 3924.
(12) Pattnaik, P. *Appl. Biochem. Biotechnol.* **2005**, *126*, 79.
(13) Sackmann, E. *Science* **1996**, *271*, 43.
(14) van Oudenaarden, A.; Boxer, S. G. *Science* **1999**, *285*, 1046.
(15) Groves, J. T.; Boxer, S. G.; McConnel, H. M. *Proc. Natl. Acad. Sci. U.S.A.* **1997**, *94*, 13390.
(16) Daniel, S.; Diaz, A. J.; Martinez, K. M.; Bench, B. J.; Albertorio, F.; Cremer, P. S. *J. Am. Chem. Soc.* **2007**, *129*, 8072.
(17) Neumann, J.; Hennig, M.; Wixforth, A.; Manus, S.; Radler, J. O.; Schneider, M. F. *Nano Lett.* **2010**, *10*, 2903.
(18) Jonsson, P.; Gunnarsson, A.; Hook, F. *Anal. Chem.* **2011**, *83*, 604.
(19) Cho, N. J.; Frank, C. W.; Kasemo, B.; Hook, F. *Nat. Protoc.* **2010**, *5*, 1096.
(20) Keller, C. A.; Kasemo, B. *Biophys. J.* **1998**, *75*, 1397.
(21) Nollert, P.; Kiefer, H.; Jahnig, F. *Biophys. J.* **1995**, *69*, 1447.
(22) Zhdanov, V. P.; Kasemo, B. *Langmuir* **2001**, *17*, 3518.
(23) Sundh, M.; Svedhem, S.; Sutherland, D. S. *Phys. Chem. Chem. Phys.* **2010**, *12*, 453.
(24) Seantier, B.; Breffa, C.; Felix, O.; Decher, G. *Nano Lett.* **2004**, *4*, 5.
(25) Hamai, C.; Yang, T. L.; Kataoka, S.; Cremer, P. S.; Musser, S. M. *Biophys. J.* **2006**, *90*, 1241.
(26) Graneli, A.; Rydstrom, J.; Kasemo, B.; Hook, F. *Langmuir* **2003**, *19*, 842.
(27) Dodd, C. E.; Johnson, B. R. G.; Jeuken, L. J. C.; Bugg, T. D. H.; Bushby, R. J.; Evans, S. D. *Biointerphases* **2008**, *3*, FA59.
(28) Ramirez, D. M. C.; Ogilvie, W. W.; Johnston, L. J. *Biochim. Biophys. Acta, Biomembr.* **2010**, *1798*, 558.
(29) Reich, C.; Horton, M. R.; Krause, B.; Gast, A. P.; Radler, J. O.; Nickel, B. *Biophys. J.* **2008**, *95*, 657.
(30) Tanaka, M.; Kaufmann, S.; Nissen, J.; Hochrein, M. *Phys. Chem. Chem. Phys.* **2001**, *3*, 4091.
(31) Kam, L.; Boxer, S. G. *J. Am. Chem. Soc.* **2000**, *122*, 12901.
(32) Janshoff, A.; Kunneke, S. *Eur. Biophys. J.* **2000**, *29*, 549.
(33) Jonsson, P.; Beech, J. P.; Tegenfeldt, J. O.; Hook, F. *J. Am. Chem. Soc.* **2009**, *131*, 5294.
(34) Jonsson, P.; Jonsson, M. P.; Tegenfeldt, J. O.; Hook, F. *Biophys. J.* **2008**, *95*, 5334.
(35) Jonsson, P.; Beech, J. P.; Tegenfeldt, J. O.; Hook, F. *Langmuir* **2009**, *25*, 6279.
(36) Hamai, C.; Cremer, P. S.; Musser, S. M. *Biophys. J.* **2007**, *92*, 1988.
(37) Lipowsky, R.; Seifert, U. *Mol. Cryst. Liq. Cryst.* **1991**, *202*, 17.
(38) Buckley, N. E.; Matyas, G. R.; Spiegel, S. *Exp. Cell. Res.* **1990**, *189*, 13.
(39) Borch, J.; Torta, F.; Sligar, S. G.; Roepstorff, P. *Anal. Chem.* **2008**, *80*, 6245.
(40) Tanaka, M.; Wong, A. P.; Rehfeldt, F.; Tutus, M.; Kaufmann, S. *J. Am. Chem. Soc.* **2004**, *126*, 3257.
(41) Chughtai, K.; Heeren, R. M. A. *Chem. Rev.* **2010**, *110*, 3237.
(42) Jonsson, P.; Jonsson, M. P.; Hook, F. *Nano Lett.* **2010**, *10*, 1900.

NOTE ADDED AFTER ASAP PUBLICATION

The third co-author was added after initial publication and was reposted August 17, 2011.